Metal-Free Multi-Porous Carbon for Electrochemical Energy Storage and Electrocatalysis Applications

Deviprasath Chinnadurai[a], Pandi Karuppiah[b], Shen-Ming Chen[b]*, Hee-jee Kim[a], Kandasamy Prabakar [a]*

[a]Department of Electrical and Computer Engineering, Pusan National University, 2 Busandaehak-ro 63beon-gil, Geumjeong-Gu, Busan-46241, Republic of Korea.

[b]Department of Chemical Engineering and Biotechnology, National Taipei University of Technology, Taipei, 10608, Taiwan
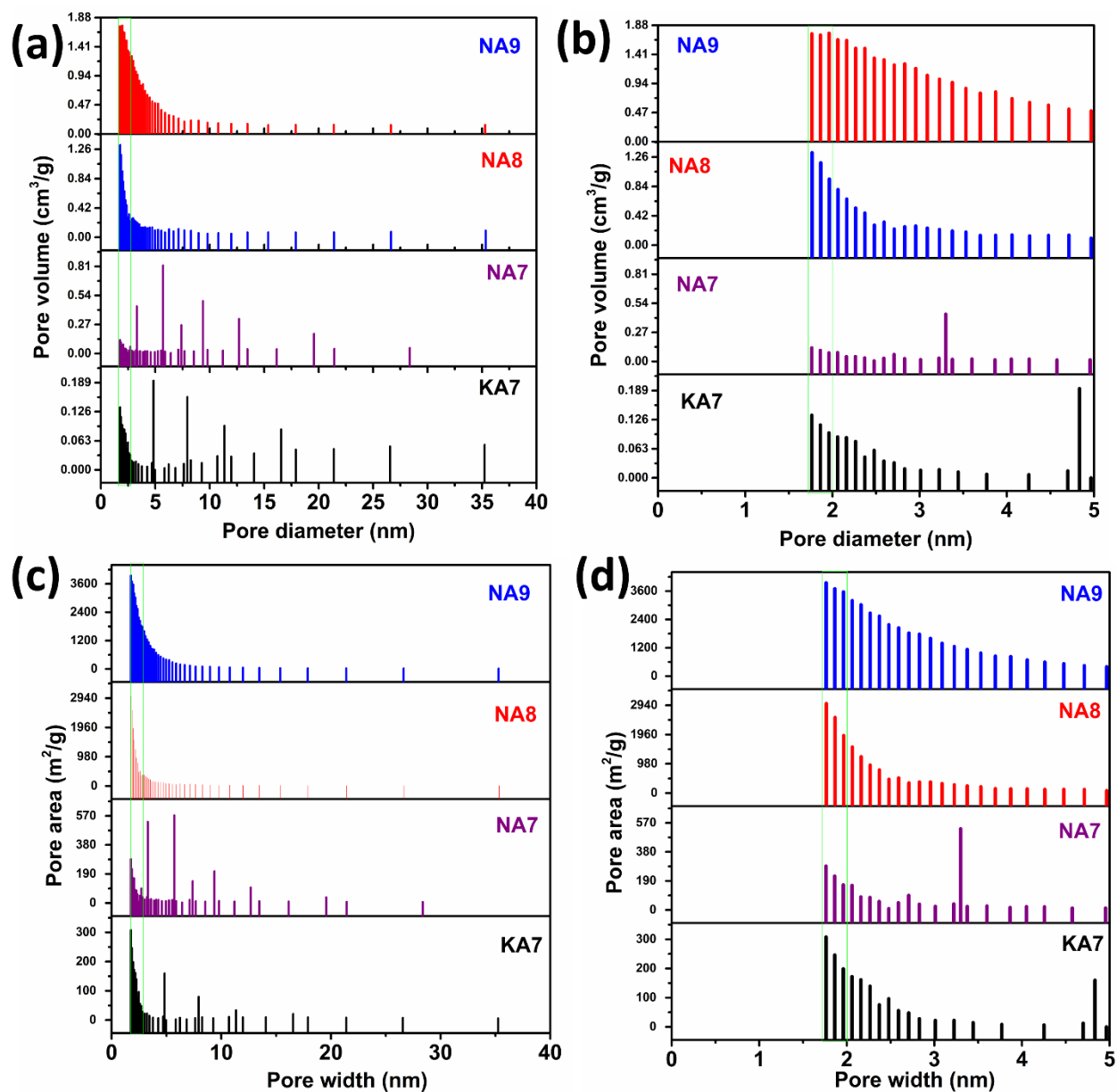
Figure S1. Pore size distribution graphs by BJH method obtained from BET analysis.

The pore size distribution graphs with respect to pore volume and pore area is given in Figure S1 for understating the pore arrangements in carbon samples. NA8 and NA9 have a higher concentration of pores in the region of 1.7 to 5 nm which results in higher surface area where as NA7 and KA7 are having very less pore density and pore area and hence have lower surface area.
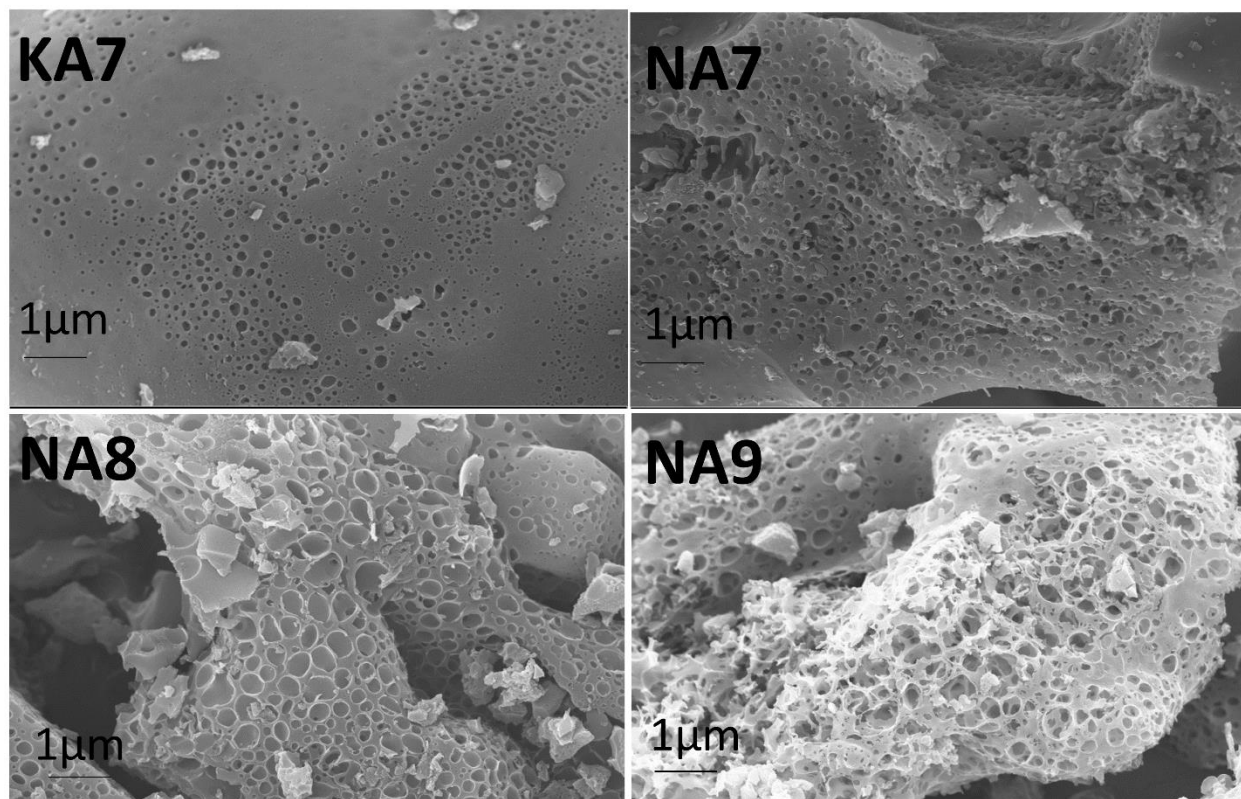
Figure S2. Low magnification FE-SEM images of carbon samples prepared at a various temperature

The low magnification FE-SEM images of the samples prepared at different temperatures show

the distribution of pore density and size having honeycomb-like morphology.
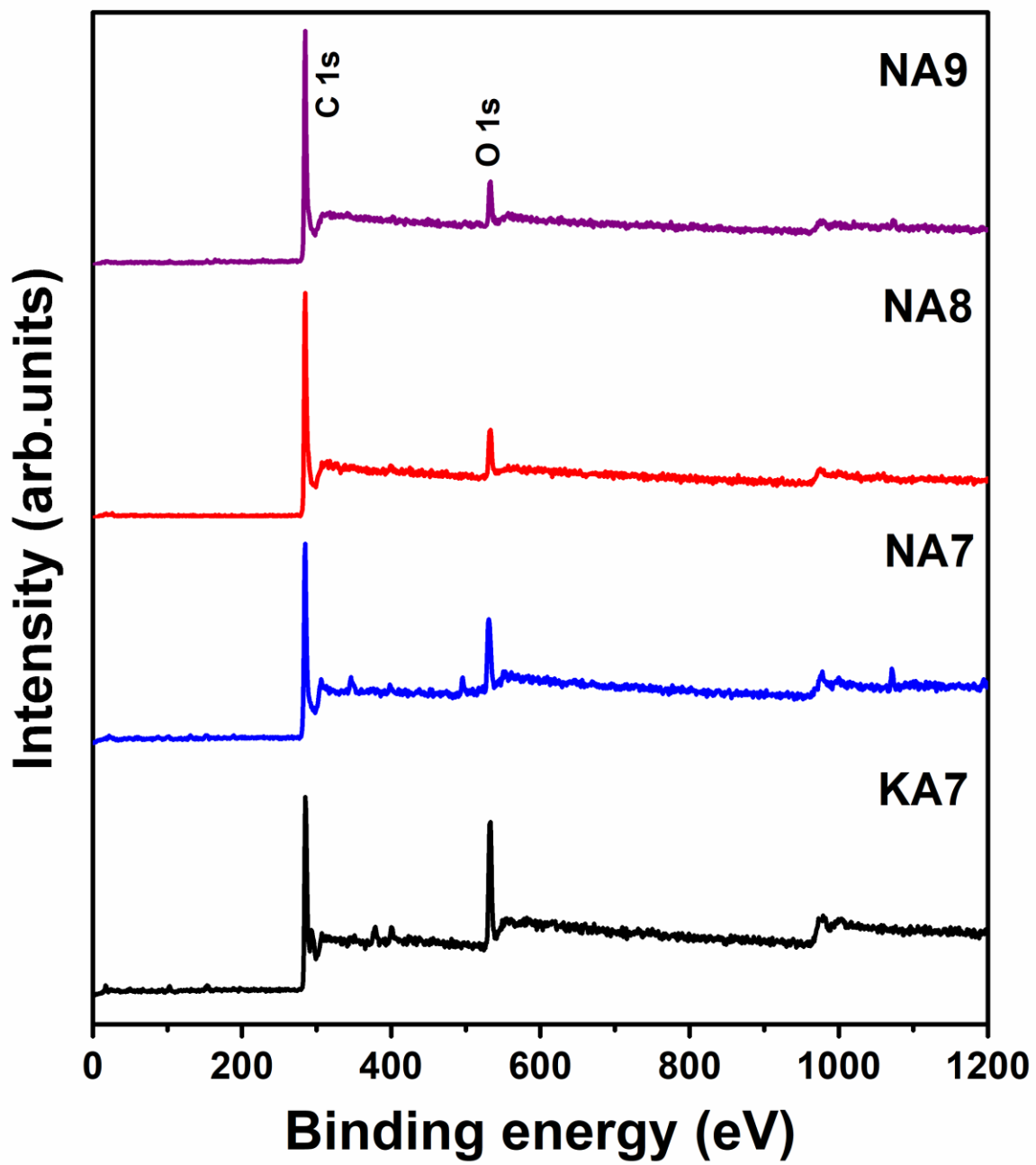
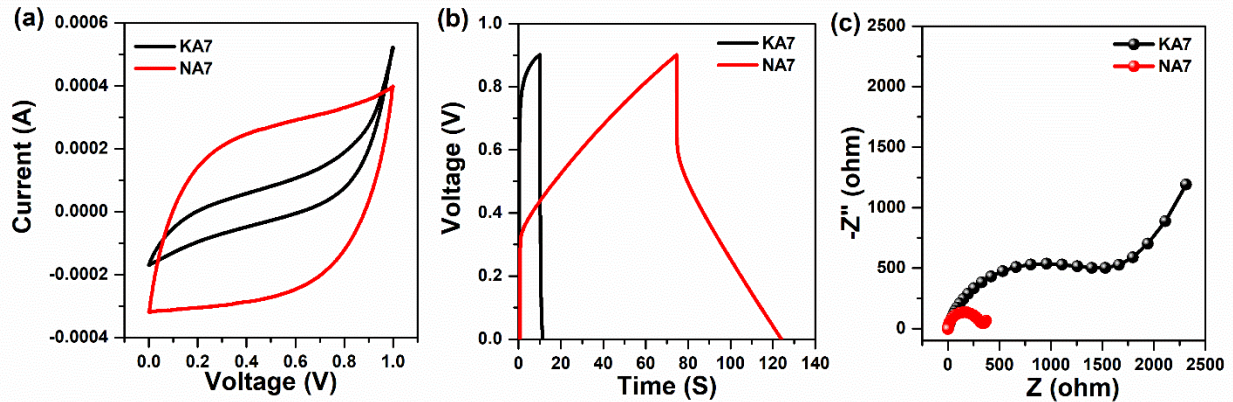**Figure S3**. XPS survey spectra of as prepared carbon samples.

Figure S4. (a) CV curves (b) GCD curves (c) EIS spectra of KA7 and NA7 samples

A comparative electrochemical study has been conducted for the samples activated in NaOH and KOH. The CV curves in Figure S4 clearly show that the samples activated in NaOH exhibit a larger area and perfect rectangular shape. Figure S4 b shows the GCD graph evidence that the sample activated in NaOH show enhance charging/discharging time. Figure S4 c shows the EIS analysis curves from which we could clearly see that the NaOH activated sample (NA7) is having very low contact resistance. Hence, NaOH was further used to characterize and OER and HER characterization.
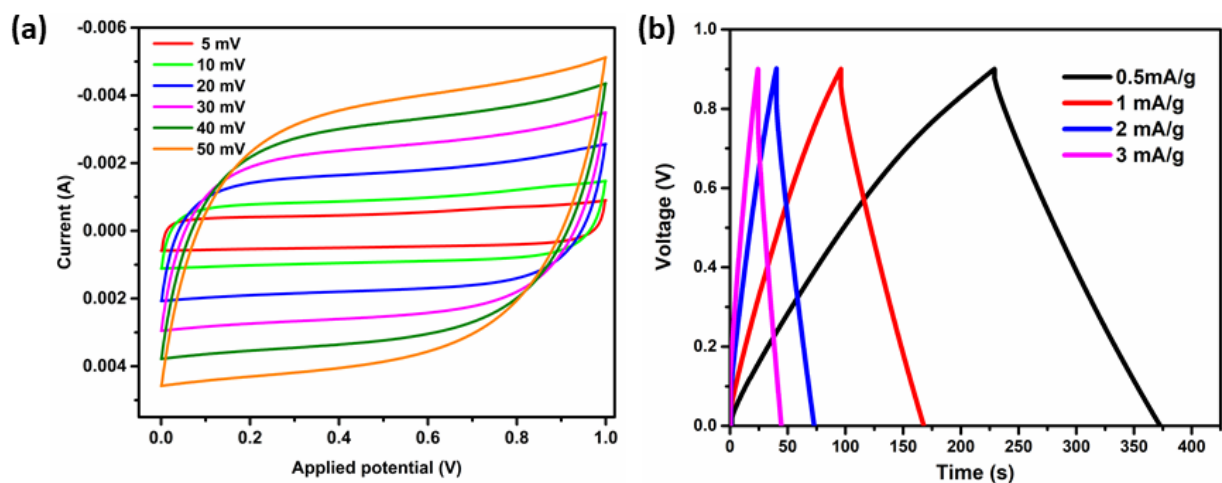
Figure S5. (a)) CV at a various scan rate and (b) GCD curves at various current density for NA9 device

Figures S5 a, shows the CV graph for sample NA9 at different scan rates. The rectangular shape of the CV curve is retained even at the higher scan rate. Figure S5 b shows the GCD curve of NA9 proves the symmetrical charging/discharging of the device at the different applied current rate.
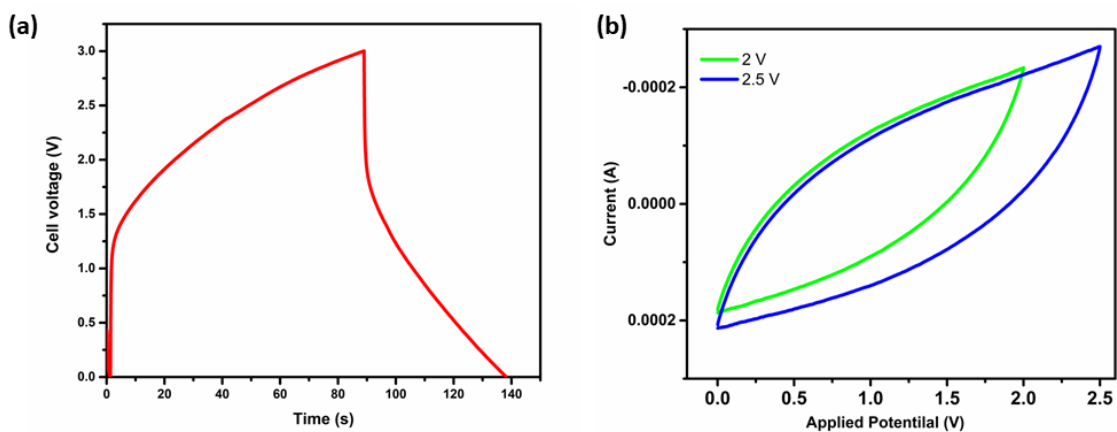

Figure S6. (a) The CV and (b) GCD curve for three NA9 supercapacitor devices connected in series.

The CV and GCD curves of three supercapacitor devices connected in series are given in Figure S6 a and b respectively.

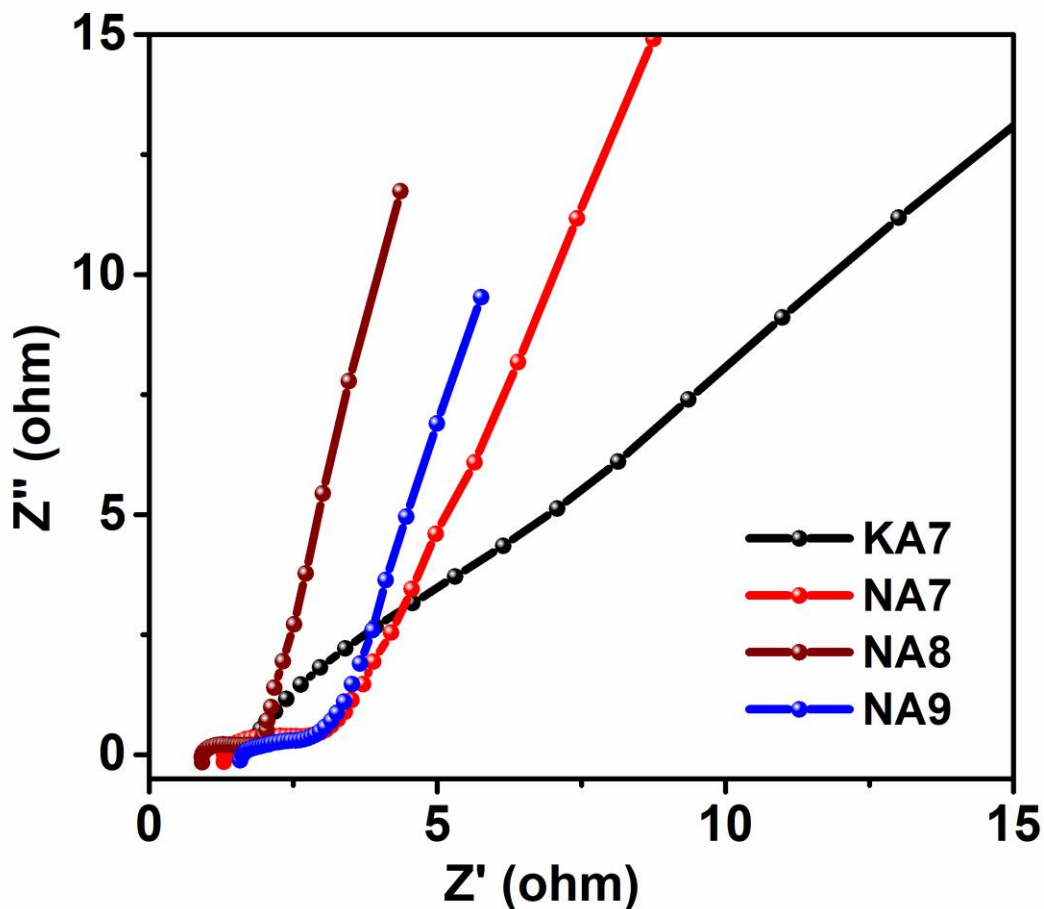**Figure S7.** EIS curves of carbon samples in 1M KOH prior to OER and HER studies.

The EIS curve of the prepared electrode for OER and HER   applications has been given in Figure S7

Electrochemical calculations for symmetric supercapacitors.

1) The gravimetric specific capacitance for a single electrode was calculated from the Galvanostatic charge-discharge profile using the formula (1)

$$C_{sp} = \frac{2I}{(dV/dt)m} \qquad (1)$$

Where I is the current (A), dV/dt is the slope of the discharge curve without ohmic loss and m is the mass in gram of the active material in an electrode

The Energy density (E, Whkg^{-1}) and power density (P, Wkg^{-1}) was calculated from equations (2) and (3) given below

$$E = \frac{1}{2}.C_{sp}.V^2.\frac{1}{4}.\frac{1}{3.6} \qquad (2)$$

$$P = \frac{E}{t}.3600 \qquad (3)$$

Where V is the cell voltage after the ohmic drop (V) and t is the discharge time (h).

Table S1: Composition of elements calculated from the XPS survey spectra

Sample name	C (%)	O (%)	N (%)	K (%)	Na (%)
KA7	71.1	20.7	4.5	3.7	-
NA7	72.7	19.5	4.4	-	3.4
NA8	87.3	10.1	2.6	-	-
NA9	87.7	10.3	< 1	-	-

Table S2: The deconvoluted C1s spectra and the composition of species bonded to C from XPS analysis.

Sample name	C=C (%)	C-N/C-OH (%)	C=O (%)	O-C=O (%)
KA7	68.53 %	19.23 %	6.91 %	5.27 %
NA7	78.87 %	12.44 %	5.5 %	3.09 %
NA8	78.93 %	11.18 %	5.68 %	4.21 %
NA9	82.15 %	10.25 %	4.65 %	2.94 %

Table S3. Comparison of HER and OER overpotentials for various carbon-based materials with our work.

Bifunctional catalyst	η for HER @10 mA/cm²	η for OER @10 mA/cm²	Ref.
Co/NBC nanocarbon	117	302	[1]
CoM (M=Fe, Cu, Ni) @ N -enriched carbon	202	303	[2]
Co/Ni$_3$N@N-doped carbon	68	247	[3]
FeCo @ Nitrogen-doped graphite/carbon nanotube	332	450	[4]
CoP @ N-doped 2D carbon sheets	71	313	[5]
CoP Nanoparticle-Embedded N-Doped Carbon Nanotube Hollow Polyhedron	140	310	[6]
3D N-doped carbon-@ core-shell metal oxides/phosphides	237	285	[7]
CoP nanoparticles encapsulated in N, P, and S tri-doped porous carbon	93	326	[8]
Nitrogen-Doped Carbon Nanosheets	392	381	[9]
Carbon derived from zeolitic imidazolate frameworks	155	476	[10]
Honeycomb carbon	184	301	This work

References

1. L. Mei-Rong, H. Qin-Long, L. Qiao-Hong, D. Yonghua, Z. Hai-Xia, C. Shumei, Z. Tianhua and Z. Jian, *Advanced Functional Materials*, 2018, **28**, 1801136.
2. X. Feng, X. Bo and L. Guo, *Journal of Power Sources*, 2018, **389**, 249-259.
3. C. Ray, S. C. Lee, B. Jin, A. Kundu, J. H. Park and S. Chan Jun, *Journal of Materials Chemistry A*, 2018, **6**, 4466-4476.
4. B. Du, Q.-T. Meng, J.-Q. Sha and J.-S. Li, *New Journal of Chemistry*, 2018, **42**, 3409-3414.
5. T. Yin, X. Zhou, A. Wu, H. Yan, Q. Feng and C. Tian, *Electrochimica Acta*, 2018, **276**, 362-369.
6. Y. Pan, K. Sun, S. Liu, X. Cao, K. Wu, W.-C. Cheong, Z. Chen, Y. Wang, Y. Li, Y. Liu, D. Wang, Q. Peng, C. Chen and Y. Li, *Journal of the American Chemical Society*, 2018, **140**, 2610-2618.
7. Q. Hu, X. Liu, C. Tang, L. Fan, X. Chai, Q. Zhang, J. Liu and C. He, *Sustainable Energy & Fuels*, 2018, **2**, 1085-1092.

8.   Y. Hu, F. Li, Y. Long, H. Yang, L. Gao, X. Long, H. Hu, N. Xu, J. Jin and J. Ma, *Journal of Materials Chemistry A*, 2018, **6**, 10433-10440.

9.   J.-J. Lv, Y. Li, S. Wu, H. Fang, L.-L. Li, R.-B. Song, J. Ma and J.-J. Zhu, *ACS Applied Materials & Interfaces*, 2018, **10**, 11678-11688.

10.   Y. Lei, L. Wei, S. Zhai, Y. Wang, H. E. Karahan, X. Chen, Z. Zhou, C. Wang, X. Sui and Y. Chen, *Materials Chemistry Frontiers*, 2018, **2**, 102-111.